Ecological Modelling 475 (2023) 110203

Contents lists available at ScienceDirect

Ecological Modelling

journal homepage: www.elsevier.com/locate/ecolmodel

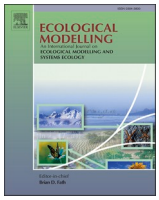

Chaos does not drive lower synchrony for intrinsically-induced population fluctuations

Guenchik Grosklos [1,*], Jia Zhao

Department of Mathematics and Statistics, Utah State University, 3900 Old Main Hill, Logan, UT 84322, USA

ARTICLE INFO

Keywords:
Metapopulation dynamics
Chaos
Metapopulation synchrony
Dispersal

ABSTRACT

Amphibians naturally occur in metapopulations characterized by spatially separated breeding habitats connected by dispersing individuals. The rate at which individuals grow to maturity, size of the metapopulation, and movement behavior varies widely across amphibian species, and their compounding interactions play a large role in population dynamics and viability. When populations in a connected network exhibit cyclic behavior the level of synchrony between populations is important for assessing extinction risk. In addition, the qualitative behavior of fluctuations provides insight into the patterns of the population cycles and can be used to predict forward trajectories in time. Chaotic oscillations, characterized by aperiodic cycles and sensitivity to initial conditions, are known to amplify noise, thus lowering population synchrony; however, other oscillation types (invariant cycles, k-cycles) have not been explicitly explored in relation to synchrony. In this paper, we investigate the relationship between synchrony and oscillation type for a two-patch system of a species with 1, 2, and 3 life-history stages. Using dynamical systems analysis, we determine the mechanisms that induce the different oscillation types and relate them with dispersal rates and synchrony. We find that dispersal has a greater effect on population dynamics of a species with 1 life-history stage compared to the subtle changes in dynamics found for species with 2 and 3 life-history stages. For low levels of dispersal, oscillating populations are driven to equilibrium as synchrony increases. Under medium to high levels of dispersal, oscillations may be created from equilibrium with low levels of synchrony. In general, chaos does not have noticeably lower synchrony than other oscillation types but has synchrony levels comparable to the oscillation types surrounding chaos. In this study, we cover a broad range of dispersal probabilities and life histories intended for general amphibian systems. The variety of results found in our analysis emphasizes the importance of determining model parameters and life history assumptions when studying specific amphibian species to ensure that the resulting dynamics accurately reflect the system.

1. Introduction

Many species live in isolated habitats as part of a spatially structured population, or metapopulation. In these systems, organisms within the habitats, or patches, experience demographic processes (fecundity, growth, etc.) independent of proximal patches while dispersal allows for interpatch interactions. The consequences of these interactions vary and can range from inducing rescue effects in low quality patches to increasing global extinction risk through hyper-synchronization (Abbott 2011; Hudson and Cattadori 1999; Ylikarjula et al. 2000). Additionally, dispersal may induce changes to the global metapopulation, including qualitative shifts in population dynamics (e.g., oscillating versus non-oscillating populations), and synchrony (Abbott 2011; Doebeli 1995; Gyllenberg et al. 1992; Hastings 2004; Ives et al. 2003; Wang and Loreau 2014; Ylikarjula et al. 2000). The relationship between dispersal, population dynamics, and synchrony play an important role in assessing population viability for both local and global populations.

The degree to which populations fluctuate in the same direction, i.e., synchrony, has important implications for population persistence. Highly synchronous populations pose a greater risk for global extinction, whereas asynchronous populations are more robust to negative

* Corresponding author.
E-mail address: guen.grosklos@speedgoat.io (G. Grosklos).
[1] Present address: Wildlife Biology Program, Department of Ecosystem and Conservation Sciences, W.A. Franke College of Forestry and Conservation, University of Montana, Missoula, Montana, 59812, USA.

https://doi.org/10.1016/j.ecolmodel.2022.110203
Received 15 June 2022; Received in revised form 19 October 2022; Accepted 2 November 2022
Available online 11 November 2022

environmental effects (Allen et al. 1993; Heino et al. 1997). Two well-known drivers of population synchrony are dispersal and environmental variability (Abbott 2011; Hudson and Cattadori 1999). In other words, subpopulations within a connected network may fluctuate in the same direction when the connection between them is strong, or, for less connected systems, fluctuations may be driven by changes in the environment, i.e., the Moran effect (Moran 1953). It is generally assumed that dispersal is the main cause for synchrony on a local scale, but the Moran effect has a greater impact on synchrony when patches are far apart and dispersal between them is limited (Hudson and Cattadori 1999).

Many studies have focused on the relationship between dispersal, synchrony, and oscillating populations defined by their variance (Abbott 2011; Allen et al. 1993; Jansen 1999; Wang et al. 2015). Generally, low levels of dispersal may initially synchronize populations while reducing variance, whereas moderate to high levels of dispersal may desynchronize populations while increasing variance (Abbott 2011; Bjørnstad et al. 1999; Dey et al. 2014; Jansen 1999; Kendall and Fox 1998). In these studies, variance is used to measure population dynamics; however, the qualitative behavior of oscillations are largely ignored. Oscillation types reveal patterns in the population that can be used to predict expected dynamics and the mechanisms driving that behavior. Where many oscillation types have smooth curves and predictable trajectories, chaotic oscillations are of particular interest due to their seemingly random dynamics and robustness to negative environmental impacts (Allen et al. 1993; Heino et al. 1997; Ranta et al. 1998). Chaos is generally associated with low synchrony populations under minimal dispersal (Allen et al. 1993; Heino et al. 1997; Ranta et al. 1998); however, other studies have observed high synchrony chaos under intermediate levels of dispersal (Udwadia and Raju 1998; Ylikarjula et al. 2000). Understanding synchrony in relation to chaos and other oscillation types can elucidate some of the mechanisms that affect synchrony, and subsequently persistence, in fluctuating populations.

Pond-breeding amphibians are excellent for studying metapopulation dynamics. They begin their lives as fully aquatic larvae with waterbody-specific survival. Larvae quickly develop into juveniles within the first year and may reach sexual maturity anywhere from one to six years of age (Bull 2005; Halley et al. 1996; McCaffery et al. 2012; Patla and Keinath 2005; Reaser 2000; Vonesh and De la Cruz 2002). In post-larval stages, individuals are capable of dispersing between patches for breeding, seeking favorable habitats, or escaping predation (Boualit et al. 2019; Buxton and Sperry 2017; Cayuela et al. 2018; Gamble et al. 2007; Tournier et al. 2017). Due to the difficulty in reliably tracking individuals, movement behavior is largely unknown, but could be driven by factors such as landscape type, social behavior, and proximity to other breeding sites (Bowler and Benton 2005; Bull 2005; Cayuela et al. 2020; Ross et al. 1999; Semlitsch 2010). Amphibians are not known to be long-distance dispersers, but evidence shows that they may travel multiple kilometers to seek new habitat (Cayuela et al. 2020; Funk et al. 2005). The consequences of amphibian dispersal vary, and include population rescue through colonization, increased genetic variation, and complex dynamics induced by eco-evolutionary feedback loops (Cayuela et al. 2020).

Mathematical models are used to understand amphibian life histories, growth rates, dispersal, and processes driving population dynamics. Because of the discrete nature of amphibian life cycles, matrix models are used with body sizes discretized into multiple life-history stages (Biek et al. 2002; Halley et al. 1996; Hellriegel 2000; McCaffery and Maxell 2010; McCaffery et al. 2012; 2014; Vonesh and De la Cruz 2002). The number of life-history stages used differ between species, and describe the time required for newborns to reach sexual maturity. Individuals may develop into breeding adults after the first year of survival, or undergo intermediate life-history changes as terrestrial, yet non-breeding individuals (Halley et al. 1996; Hellriegel 2000; McCaffery et al. 2012; 2014; Vonesh and De la Cruz 2002; Willson et al. 2012; Willson and Hopkins 2013). Breeding waterbodies are discretely defined to describe site-specific larval survival with resource regulation that allows for complex dynamics in the system (Halley et al. 1996; Hellriegel 2000; Vonesh and De la Cruz 2002; Willson et al. 2012).

In this paper, we explore the effects of dispersal on the dynamics of a two-patch model of a species with 1, 2, or 3 life-history stages. We investigate the relationship between oscillation type, synchrony, and dispersal while identifying the mechanisms driving oscillations. Our models are parameterized using amphibian literature characterized by discrete life-history stage development, high fecundity, and low larval survival (McCaffery et al. 2014; Vonesh and De la Cruz 2002; Willson and Hopkins 2013). This work offers a new perspective on the relationship between synchrony and population fluctuations by explicitly identifying the different oscillation types induced by dispersal under a broad range of dispersal probabilites and life history demographics. Although posed as a general model for amphibian systems, the methods used in this paper can be used to motivate model development and analysis for specific amphibian systems.

2. Methods

2.1. The one-patch model

Local patches without dispersal are used to understand how populations behave independent of all other patches. We define models of a species with 1, 2, and 3 life-history stages. Models with one life-history stage assume that individuals develop into breeding adults within the first year (Halley et al. 1996). Models with two life-history stages assume that individuals develop into non-breeding juveniles before reaching maturation (Hellriegel 2000; Vonesh and De la Cruz 2002). Models with three life-history stages assume an intermediate subadult stage where individuals are non-breeding but have demographies similar to breeding adults (McCaffery et al. 2012; 2014). For a species with n life-history stages, population vectors are defined as

$$\boldsymbol{u}_1 = [a], \text{ when n} = 1, \tag{1a}$$

$$\boldsymbol{u}_2 = \begin{bmatrix} j \\ ma \end{bmatrix}, \text{ when n} = 2, \tag{1b}$$

$$\boldsymbol{u}_3 = \begin{bmatrix} j \\ s \\ a \end{bmatrix}, \text{ when n} = 3, \tag{1c}$$

where j, s, and a are the juvenile, subadult, and adult densities.

Local patch demographics are defined using $n \times n$ matrices that describe interactions between individuals. For a single-stage population, new recruits mature into breeding adults (a) after surviving their first year. The demographic matrix is defined as

$$\boldsymbol{B}_1 = [S_a + FH_a], \tag{2}$$

with corresponding population vector $\mathbf{u}_1$ defined in (1a), S_a is the survival probability of adults, F is the fecundity rate, and H_a is the density-dependent first-year survival (see Section 2.1.1). The fecundity term includes adult breeding probability, clutch size, and egg survival.

For a 2-stage population, new recruits grow into juveniles (j) in their first year then have some probability of transitioning to breeding adults in subsequent years. The demographic matrix is defined as

$$\boldsymbol{B}_2 = \begin{bmatrix} S_j(1 - P_{ja}) & FH_a \\ S_j P_{ja} & S_a \end{bmatrix}, \tag{3}$$

with corresponding population vector $\mathbf{u}_2$ defined in (1b), P_{ja} is the probability of transitioning from the juvenile to adult stage, and S_j is the survival probability of juveniles.

Finally, a 3-stage population assumes an intermediate non-breeding stage (subadults; s) with survival probabilities similar to adults. We assume that individuals may only transition to latter stages in single-stage

increments. The demographic matrix is defined as

$$\boldsymbol{B}_3 = \begin{bmatrix} S_j(1-P_{js}) & 0 & FH_a \\ S_jP_{js} & S_s(1-P_{sa}) & 0 \\ 0 & S_sP_{sa} & S_a \end{bmatrix}, \tag{4}$$

with corresponding population vector $\mathbf{u}_3$ defined in (1c), P_{js} and P_{sa} are transition probabilities from juvenile to subadult and subadult to adult, and S_s is the survival probability of subadults.

Local populations are projected forward in time by multiplying the demographic matrix with the population vector,

$$\mathbf{u}_n(t+1) = \mathbf{B}_n\mathbf{u}_n(t). \tag{5}$$

2.1.1. Nonlinear larval survival

In each patch, we assume negative density-dependent survival in first-year individuals to represent larval competition. We use the Hassell competition model to define first-year survival based on the number of breeding adults in the same year (Halley et al. 1996; Vonesh and De la Cruz 2002; Willson et al. 2012; Willson and Hopkins 2013),

$$H_a = \frac{L}{\left(1 + \frac{Fa}{K}\right)^{\gamma}}, \tag{6}$$

where L is the maximum first-year survival, K is the carrying capacity, and γ is the densitydependent exponent. Other forms of density-dependent survival have been used in amphibian models including the Ricker model (Hellriegel 2000) and Gompertz model (Băncilă et al. 2016; Bendik and Dries 2018). We choose the Hassell competition model because of its realism and use in multiple amphibian studies (Halley et al. 1996; Vonesh and De la Cruz 2002; Willson et al. 2012; Willson and Hopkins 2013).

Competition in the Hassell equation depends on the density-dependent exponent, γ, where γ is inversely proportional to patch size (Anazawa 2019). For smaller values of γ, individuals undergo 'contest' competition while for large values of γ, individuals undergo 'scramble' competition (Hassell 1975). In contest competition, some proportion of the individuals receive sufficient resources for survival while the rest do not survive. In scramble competition, all resources are 'shared' such that individuals either all die out or all survive. For extreme cases, ideal contest competition ($\gamma = 1$) defines the Ricker model while ideal scramble competition ($\gamma \to \infty$), defines the Beverton-Holt model (Anazawa 2019).

2.2. The two-patch model

Given a metapopulation with two patches and n life-history stages, we define a patch-based population vector $\mathbf{u}_n(t) \in \mathrm{R}^{2n}$ as

$$\mathbf{u}_n(t) = \begin{bmatrix} \boldsymbol{u}_{1n}(t) \\ \boldsymbol{u}_{2n}(t) \end{bmatrix}, \tag{7}$$

where $\mathbf{u}_{xn}(t) \in \mathrm{R}^n$, $x = 1,2$, is a subvector of length n and represents population distributions for n life-history stages in patch x at time t.

We define a two-patch, n-stage model where each patch experiences demographic processes independent of the other patch and interactions between them occur through a dispersal mechanism. The projection matrix $\mathbf{A}_n \in \mathrm{R}^{2n,2n}$ is defined as

$$\boldsymbol{A}_n = \begin{bmatrix} (1-\boldsymbol{\sigma}_{1n})\boldsymbol{B}_{1n} & \boldsymbol{\sigma}_{2n}\boldsymbol{B}_{2n} \\ \boldsymbol{\sigma}_{1n}\boldsymbol{B}_{1n} & (1-\boldsymbol{\sigma}_{2n})\boldsymbol{B}_{2n} \end{bmatrix}, \tag{8}$$

where $\boldsymbol{\sigma}_{xn} \in \mathrm{R}^{n,n}$ is a diagonal matrix with entries that represent dispersal probabilities for n life-history stages from patch $x = 1,2$, and $\mathbf{B}_{xn} \in \mathrm{R}^{n,n}$ is the demographic matrix for patch $x = 1,2$. The diagonal submatrices in $\mathbf{A}_n$, $(1 - \sigma_{xn})\mathbf{B}_{xn}$, represent demographic processes of individuals who remain in patch x while the off-diagonal submatrices, $\boldsymbol{\sigma}_{xn}\mathbf{B}_{xn}$, represent demographic and dispersal processes of individuals dispersing from patch x.

With the notations above, the two-patch model with multiple life-history stages is expressed as

$$\mathbf{u}_n(t+1) = \mathbf{A}_n\mathbf{u}_n(t). \tag{9}$$

2.3. Eigenvalue analysis and population stability

We use linearization techniques evaluated at equilibrium to determine local stability of fixed points and identify oscillation types using Lyapunov exponents. Fixed points are found by setting $j(t+1) = j(t) = j^*$, $s(t+1) = s(t) = s^*$, and $a(t+1) = a(t) = a^*$ for the appropriate model and stability is determined by analyzing the dominant eigenvalue, λ, of the Jacobian matrix evaluated at the fixed point. The magnitude of the dominant eigenvalue determines whether the fixed point is stable ($|\lambda| < 1$) or unstable ($|\lambda| > 1$). For stable fixed points ($|\lambda| < 1$), asymptotic behavior of populations that start near the fixed point will converge to the fixed point. Additionally, convergence to an equilibrium may occur monotically when the dominant eigenvalue is real (node), or non-monotically when the dominant eigenvalue contains a nonzero imaginary part (spiral). For unstable fixed points ($|\lambda| > 1$), nearby trajectories are repelled from the fixed point and will converge to the nearest attractor. Oscillations occur when the dominant eigenvalue does not have an imaginary part and is less than -1, or the imaginary part of the dominant eigenvalue is nonzero and $|\lambda| > 1$. We classify oscillations into three attractor types (invariant cycles, k-cycles, and chaos) based on the calculated Lyapunov exponent (see Section 2.5).

2.4. The Jacobian matrix

We define Jacobians for any time t to allow for temporal analyses. Because the only density-dependent term is in the larval stage, all Jacobians have the following density dependent larval survival term,

$$\widehat{H}(t) = \frac{R_H}{\left(1 + \frac{Fa(t)}{K}\right)^{\gamma}} - \frac{\gamma F R_H}{K\left(1 + \frac{Fa(t)}{K}\right)^{\gamma+1}} a(t), \tag{10}$$

where $R_H = FL$ represents yearly recruitment rate.

The Jacobians are then defined as for the 1-stage model,

$$\mathbf{J}_1(\mathrm{t}) = \mathrm{S_a} + \widehat{H}(\mathrm{t}), \tag{11}$$

for the 2-stage model,

$$\boldsymbol{J}_2(t) = \begin{bmatrix} S_j(1-P_{ja}) & \widehat{H}(t) \\ S_jP_{ja} & S_a \end{bmatrix}, \tag{12}$$

and for the 3-stage model,

$$\boldsymbol{J}_3(t) = \begin{bmatrix} S_j(1-P_{js}) & 0 & \widehat{H}(t) \\ S_jP_s & S_s(1-P_{sa}) & 0 \\ 0 & S_sP_{sa} & S_a \end{bmatrix}. \tag{13}$$

When evaluated at equilibrium, these Jacobians are used for local stability analysis; otherwise, long-term temporal averages over the Jacobian are used for attractor identification (see section 2.5).

The Jacobian for the two-patch model is defined by

$$\overline{\mathbf{J}}_n(t) = \begin{bmatrix} (1-\boldsymbol{\sigma}_{1n})\mathbf{J}_{1n}(t) & \boldsymbol{\sigma}_{2n}\mathbf{J}_{2n}(t) \\ \boldsymbol{\sigma}_{1n}\mathbf{J}_{1n}(t) & (1-\boldsymbol{\sigma}_{2n})\mathbf{J}_{2n}(t) \end{bmatrix}, \tag{14}$$

where $\mathbf{J}_{xn}$ is the $n-$stage Jacobian for patch x with corresponding two-patch population vector $\mathbf{u}_{xn}$.

2.5. Attractor types

We classify oscillating populations into three attractor types: invariant cycles; k-cycles; and chaos. Invariant cycles have quasi-

periodic dynamics, characterized by iterative cycles around a smooth curve with slightly shifting rotations around a closed loop. K-cycles are classified by the number of points that occur in each period. Chaos is deterministic but has seemingly random dynamics that are sensitive to initial conditions. Attractor types are quantified using the Lyapunov exponent defined for matrix population models Caswell (2001),

$$\lambda_e = \lim_{T\to\infty}\frac{1}{T}\ln|\mathbf{J}_n(T-1)\cdots \boldsymbol{J}_n(0)\ \boldsymbol{u}_n(0)|. \tag{15}$$

Here, $\mathbf{J}_n(t)$ is the n-stage Jacobian matrix at time t, $\mathbf{u}_n(0)$ is the initial population vector, and $|\cdot|$ is the vector magnitude. Note that λ_e depends on $\mathbf{u}_n(0)$ but results remain the same with vectors in the same basin of attraction (Caswell 2001; Gyllenberg et al. 1992; Strogatz 2015). See the appendix for a demonstration of systems with fractal basins of attraction.

Oscillations are classified based on the Lyapunov exponent value where $\lambda_e < 0$ are k-cycles, $\lambda_e = 0$ are invariant cycles, and $\lambda_e > 0$, are chaos (Caswell 2001). Examples of each attractor type are summarized in Fig. 1. Because numerical simulations introduce calculation error, we identify invariant cycles if λ_e is sufficiently close to 0 (i.e., $|\lambda_e| < 0.01$). Identifying unstable dynamics without closed form eigenvalue analyses is a nontrivial task and even graphical representations of different oscillations may be ambiguous. We visually inspect selected results and find that the tolerance above sufficiently distinguishes invariant cycles from chaos and k-cycles.

Intuitively, the Lyapunov exponent measures the averaged progression of two nearby trajectories in time. If the two trajectories approach an equilibrium, the difference between them approaches 0. For oscillating populations, the difference between the two trajectories approaches 0 for in-phase k-cycles ($\lambda_e < 0$) or reaches some constant value for invariant cycles ($\lambda_e = 0$). With chaos ($\lambda_e > 0$), the trajectories never converge so the difference between them increases as time moves forward. The Jacobian matrix represents the dynamics of the deviation vector; hence, the product of all temporal Jacobian matrices describes total deviation in time.

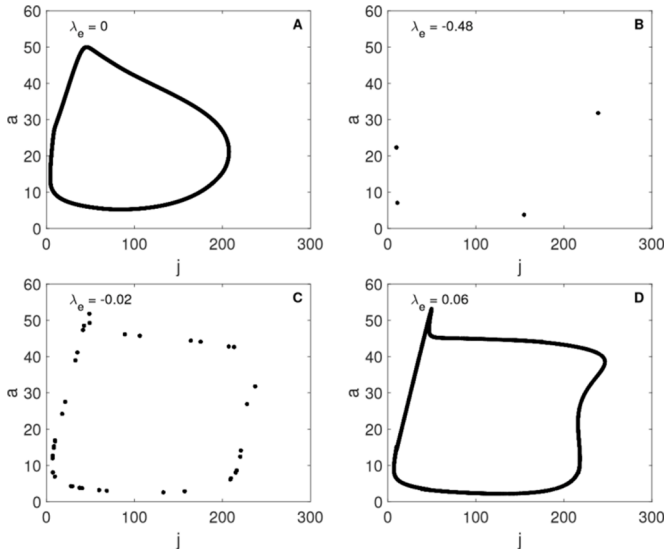

Fig. 1. Phase planes for juvenile and adult populations in the one-patch, 2-stage model with calculated Lyapunov exponent for an invariant cycle (A; $\lambda_e = 0$), low-point k-cycle (B; $\lambda_e < 0$), high-point k-cycle (C; $\lambda_e < 0$), and chaos (D; $\lambda_e > 0$). The k-cycles are formed by the phase-locked invariant cycles while retaining the shape of the closed loop. Chaos is developed as a wrinkle forms in the invariant cycle, creating sensitivity to initial conditions. Simulations are created by plotting the final 9000 juvenile and adult densities for $R_H = 167.333$, and $S_a = 0.366$(A), 0.228(B), 0.139(C), and 0.099(D).

2.6. Dispersal symmetry

We measure dispersal symmetry in two ways: (1) compare the proportion of dispersing individuals in one patch to the total proportion of dispersing individuals, and (2) partition the dispersal probability plane into zones. We use populations averaged over the final time steps $\widehat{\mathbf{u}}_{xn} = \frac{1}{500}\sum_{\tau=1}^{500}\boldsymbol{u}_{xn}(\tau)$ to define the asymmetry in per capita dispersal from each patch,

$$\alpha = \frac{\frac{N_{\sigma 1}}{N_1}}{\frac{N_{\sigma 1}}{N_1}+\frac{N_{\sigma 2}}{N_2}}, \tag{16}$$

where $N_{\sigma x} = \sum_n \boldsymbol{\sigma}_{xn}\widehat{\mathbf{u}}_{xn}$ is the number of individuals dispersing from patch $x = 1,2$, and $N_1 = \sum_n \widehat{\boldsymbol{u}}_{1n}$ is the total population size of patch 1. Dispersal is symmetric when $\alpha \approx 0.5$, and asymmetric when $\alpha \approx 0$ (mostly dispersing from patch 2) and $\alpha \approx 1$ (mostly dispersing from patch 1).

We group the dispersal plane into 5 zones that represent different dispersal probabilities and symmetries, as shown in Fig. 2. They are: low symmetric dispersal (zone 1), intermediate symmetric dispersal (zone 2), high symmetric dispersal (zone 3), low asymmetric dispersal (zone 4), and high asymmetric dispersal (zone 5). Partitioning dispersal regions into different zones provides insight into expected system dynamics based on dispersal symmetry and degree. Note that the number of simulations in each zone differs based on cover area: zones 1 and 3 have 210 simulations, zone 2 has 3260 simulations, and zones 4 and 5 have 3160 simulations.

2.7. Patch synchrony

We measure population synchrony between the two patches using patch population sizes in the final 500 time steps. This method sums over all entries in the temporal covariance matrix and divides by the square of the sum over the standard deviations (Loreau and Mazancourt 2008),

$$\beta = \frac{\sum_{i,k} cov(\widehat{\mathbf{U}}_i, \widehat{\mathbf{U}}_k)}{\left(\sum_i \sqrt{cov(\widehat{\mathbf{U}}_i, \widehat{\mathbf{U}}_i)}\right)^2}, \tag{17}$$

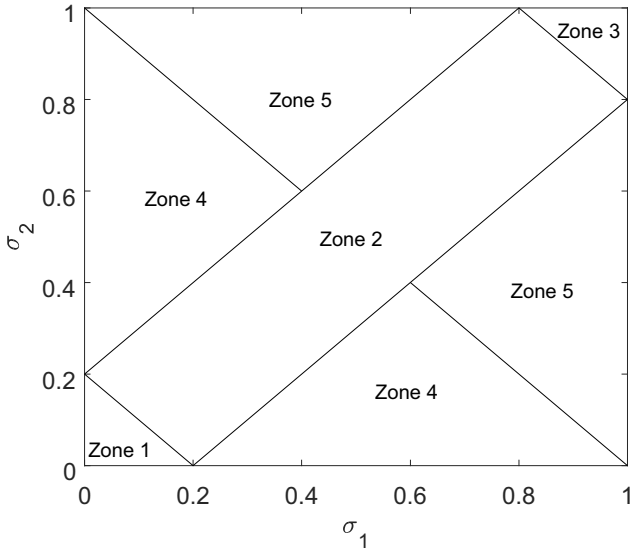

Fig. 2. The 5 zones for the dispersal plane that represent different dispersal probabilities and symmetries. Zone 1 represents low symmetric dispersal, zone 2 represents intermediate symmetric dispersal, zone 3 represents high symmetric dispersal, zone 4 represents low asymmetric dispersal, and zone 5 represents high asymmetric dispersal.

for $i = 1, 2$ and $k = 1, 2$. The vector, $\widehat{\mathbf{U}}_i$, is defined by

$$\widehat{\mathbf{U}}_i = \begin{bmatrix} \boldsymbol{U}_i(T-499) \\ \boldsymbol{U}_i(T-498) \\ \vdots \\ \boldsymbol{U}_i(T) \end{bmatrix}, \tag{18}$$

where $\boldsymbol{U}_i(t) = \sum_n \boldsymbol{u}_{in}(t)$ are patch i population sizes, and $cov(\widehat{\mathbf{U}}_i, \widehat{\mathbf{U}}_k)$are the temporal covariance measures between $\widehat{\mathbf{U}}_i$ and $\widehat{\mathbf{U}}_k$. This method measures the variance of population sizes across all patches and is standardized between 0 and 1. $\beta \approx 1$ indicates that the populations are strongly positively correlated (high synchrony) while $\beta \approx 0$ indicates that the populations are strongly negatively correlated (low synchrony). Systems with at least one stable population have perfect synchrony (only found with zero dispersal); hence even small dispersal probabilities produce cycles across all populations. Additionally, this method is robust to population magnitudes (i.e., vertical shifts in population abundances), and measures near-perfect synchrony for populations with large amplitude differences.

2.8. One-patch simulations

We investigate dynamics in the one-patch model of species with 1, 2, and 3 life-history stages by varying the range of pairwise parameter sets with all other parameters fixed. Parameters are based on estimates used in amphibian literature and we try to maintain consistent total populations across the different life-history stage models (Table 1). For each parameter combination, we first determine stability using eigenvalue analysis of the Jacobian matrix at the nontrivial fixed points. When oscillations occur, we classify the oscillation type using the Lyapunov exponent by initializing each life-history stage with 20 individuals and run simulations for $T = 10000$ time steps to ensure convergence to asymptotic behavior. The Lyapunov exponent is calculated using the final 9000 time steps to identify attractor type. Note that the carrying capacity ranges from 40000 to 80000 but time series simulations typically have populations with less than 200 individuals. Although carrying capacities seem high, the ratio between fecundity and carrying capacity (F/K) is similar to equivalent coefficients estimated in other studies (Vonesh and De la Cruz 2002; Willson et al. 2012).

2.9. Two-patch simulations

We analyze local stability of numerically solved fixed points in the two-patch model using eigenvalue analysis, and steady state behavior using Lyapunov exponents and population synchrony. Because of multiple fixed points that occur in the two-patch model, we analyze asymptotic behavior of only one trajectory using initial conditions defined in the following paragraph. Note that this does not find all alternate steady states as that requires extensive analysis of localized parameters. To account for this, we analyze a select few scenarios using bifurcation and eigenvalue analysis under multiple initial conditions to understand some of the different dynamics found in our results.

To analyze the effects of dispersal on the two-patch model, we select pairwise S_a values that initialize the model with a variety of dynamics without dispersal (see Table 2). Attractor and synchrony planes allow us to understand general system behavior while bifurcation and stability plots of fixed points for select parameter ranges provide additional information on some of the bifurcation types and alternate steady states that exist. Each simulation is initialized with steady states from the corresponding one-patch simulation. For example, in the 1-stage model, if adult survival in patch 1 is 0.1 ($S_{a1} = 0.1$) and adult survival in patch 2 is 0.7 ($S_{a2} = 0.7$) then patch 1 is initialized with one of the points on the local k-cycle while patch 2 is initialized with approximately 50 individuals corresponding to the stable equilibrium. We identify oscillations by running our models for $T = 10000$ time steps and analyzing the range of the final 50 time steps. A steady state is classified as an oscillation if the range of any population is greater than 0.01; otherwise, the steady state is an equilibrium. Attractor type is determined by calculating the Lyapunov exponent (λ_e in Eq. (15)) using the final 9000 time steps and the two-patch Jacobian defined by Eq. (14). Finally, we calculate population synchrony using patch population sizes in the final 500 time steps (see Section 2.7).

For each pair of adult survival values, we test 100 dispersal probabilities ranging from 0 to 1 for each life-history stage. With 15 pairwise adult survival probabilities and 10000 pairwise dispersal probabilities for each life-history stage, we have a total of 150,000 simulations for the 1-stage model, 300,000 simulations for the 2-stage model, and 450,000 simulations for the 3-stage model (all attractor, synchrony, and eigenvalue simulations are in the appendix).

Table 1
Default vital rates and values used in the model. Vital rates are based on ranges used in different amphibian systems.

Vital rate	Symbol	1-stage	2-stage	3-stage	Sources
Fecundity	F	500	500	500	(36)
Maximum first-year survival	L	0.2	0.2	0.2	(51; 55)
Carrying capacity	K	80000	50000	40000	(55)
Density-dependent exponent	γ	30	30	30	(51)
Juvenile survival	S_j	-	0.4	0.45	(36; 51; 55)
Subadult survival	S_s	-	-	0.7	(36)
Adult survival	S_a	0.6	0.6	0.6	(36; 51; 55)
Transition from juvenile to adult	P_{ja}	-	0.5	-	(51)
Transition from juvenile to subadult	P_{js}	-	-	0.3	(36)
Transition from subadult to adult	P_{sa}	-	-	0.6	(36)

Citations are as follows: 36-McCaffery and Maxell (2010); 51-Vonesh and De la Cruz (2002); 55-Willson et al. (2012)

3. Results

3.1. Stability analysis of the one-patch model

We vary the yearly recruitment rate, R_H, the density-dependent exponent, γ, and adult survival, S_a to understand how small parameter changes affect system dynamics. Fig. 3 shows contour plots of the calculated dominant eigenvalues for each model. The bold lines denote where bifurcations of the nontrivial steady state occur ($|\lambda| = 1$). The 1-stage model experiences flip bifurcations, causing the birth of k-cycles while the 2- and 3-stage models experience Hopf bifurcations, creating invariant cycles. Additionally, in the 3-stage model, a transcritical bifurcation occurs for low adult survival and yearly recruitment where the population experiences global extinction. This is the only region in the one-patch model where the trivial fixed point is stable.

Fig. 4 shows where different attractor types occur under the different parameter ranges. Equilibrium regions are white while oscillating regions are colored based on attractor type and k-cycle period. The

Table 2
Adult survival used in the two-patch systems with local stability dynamics and Lyapunov exponent (λ_e).

S_a	1-stage Dynamics (λ_e)	2-stage Dynamics (λ_e)	3-stage Dynamics (λ_e)
0.1	K-cycle (-0.369)	Invariant cycle (0.000)	Equilibrium (-0.003)
0.3	Chaos (0.286)	Invariant cycle (0.000)	Invariant cycle (0.000)
0.5	K-cycle (-0.356)	Invariant cycle (0.000)	Invariant cycle (0.000)
0.7	Equilibrium (-0.083)	Equilibrium (-0.060)	Equilibrium (-0.0061)
0.9	Equilibrium (-0.954)	Equilibrium (-0.083)	Equilibrium (- 0.083)

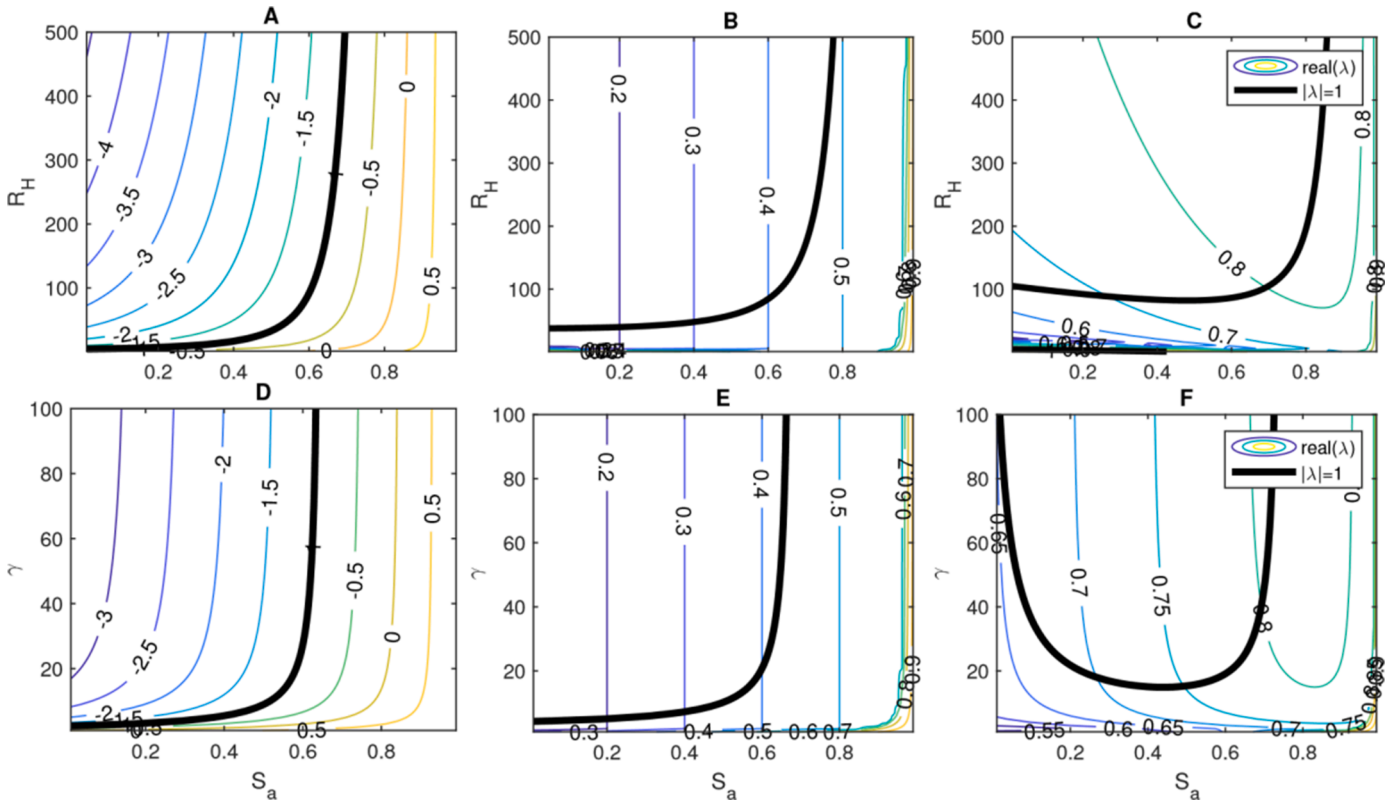

Fig. 3. Dominant eigenvalues (λ) for a range of adult survival (S_a), yearly recruitment rate (R_H), and density-dependent exponent (γ) for the one-patch model. The solid black lines represent bifurcations in the nontrivial fixed points. The 1-stage model undergoes flip bifurcations, creating k-cycles whereas the 2- and 3-stage models undergo Hopf bifurcations, inducing invariant cycles. Additionally, under low adult survival and fecundity in the 3-stage model (C), the nontrivial fixed point experiences a transcritical bifurcation where it switches stability with the trivial fixed point.

number of points in a k-cycle are numerically estimated by finding the last point in the cycle within 0.001 of the final point. We identify all 2, 4, 8, and 16 point k-cycles as well as k-cycles with periods greater than 16 (16+) and less than 16 that were not already identified (other cycles). In general, increasing the number of stages 'simplifies' the dynamics, i.e., chaos is most prevalent in the 1-stage model (A, D), a mix of dynamics are found in the 2-stage model (B, E), and invariant cycles are most prevalent in the 3-stage model (C, F). In the 1-stage model, k-cycles occur through flip bifurcations that undergo period-doubling routes to chaos. Among the chaos regions, periodic windows appear as lowpoint k-cycles. In the 2- and 3-stage models, Hopf bifurcations create invariant cycles that become phase-locked to varying degrees. Specifically, the 2-stage model has large windows of low-point cycles, high-point cycles, and chaos while the 3-stage model has fewer phase-locked regions of low-point k-cycles.

3.2. Bifurcation analysis of the one-patch model

Close inspection of bifurcation diagrams with calculated Lyapunov exponents allow us to verify results found in the eigenvalue and attractor plots. Bifurcation plots (Fig. 5A-C) are created by plotting patch 1 adults in the final 50 time steps vertically for each S_a value, and the Lyapunov exponents (Fig. 5D-F) are calculated using the final 9000 time steps. We analyze a range of adult survival values and find that a flip bifurcation occurs at $S_a \approx 0.58$ in the 1-stage model, creating k-cycles that lead to chaos through a period-doubling route. The 2- and 3-stage models experience Hopf bifurcations at $S_a \approx 0.2$ in the 3-stage model and $S_a \approx 0.6$ in the 2- and 3-stage models. Additionally, low-point phase-locked k-cycles form for a few small regions in the 2-stage model, marked by negative λ_e.

3.3. Stability and synchrony results of the two-patch model

We find that dynamics are preserved under small vital rate perturbations and dispersal may induce oscillations even if both local populations are at equilibrium. For example, the homogeneous systems in the 1-stage model ($S_{a1} = S_{a2}$) contain oscillating regions in the scenarios where both patches are at equilibrium in the absence of dispersal (B, C) and appear in similar dispersal regions as the scenario with slightly lower adult survival (A) (Fig. 6). We also find evidence of dispersal-induced oscillations for one heterogeneous scenario in the 1-stage model, $S_{a1} = 0.7$, $S_{a2} = 0.9$, three scenarios in the 2-stage model ($S_{a1} = S_{a2} = 0.7$; $S_{a1} = 0.7$, $S_{a2} = 0.9$; $S_{a1} = S_{a2} = 0.9$), and two scenarios in the 3-stage model ($S_{a1} = 0.1$, $S_{a2} = 0.7$; $S_{a1} = 0.1$, $S_{a2} = 0.9$) (see appendix). Note that dispersal-induced oscillations have only been observed under adult dispersal, presumably because of the direct effects of adults on larval-stage survival.

Fig. 7A-C shows the relative frequency of per capita symmetric dispersal (α) for each attractor type for the 1-, 2-, and 3-stage models, and Fig. 7D shows the proportion that each attractor type appears in each zone. In the 1-stage model, chaotic results (red) occur most frequently under symmetric dispersal (zones 1, 2, and 3), k-cycles (black) occur almost uniformly across different symmetries and zones, and invariant cycles (blue) occur under high dispersal (zones 3 and 5). In the 2-stage model, oscillations mostly occur under symmetric dispersal with the majority of k-cycles appearing under highly symmetric dispersal (zone 3). In the 3-stage model, invariant cycles occur under symmetric dispersal while the few instances of chaos are found in the extremes, i.e., full dispersal from one patch to the other. equilibria (purple) generally have a more uniform distribution in all three models, showing little correlation with dispersal symmetry. Note that the number of chaos events in the 2and 3-stage models are sparse compared to

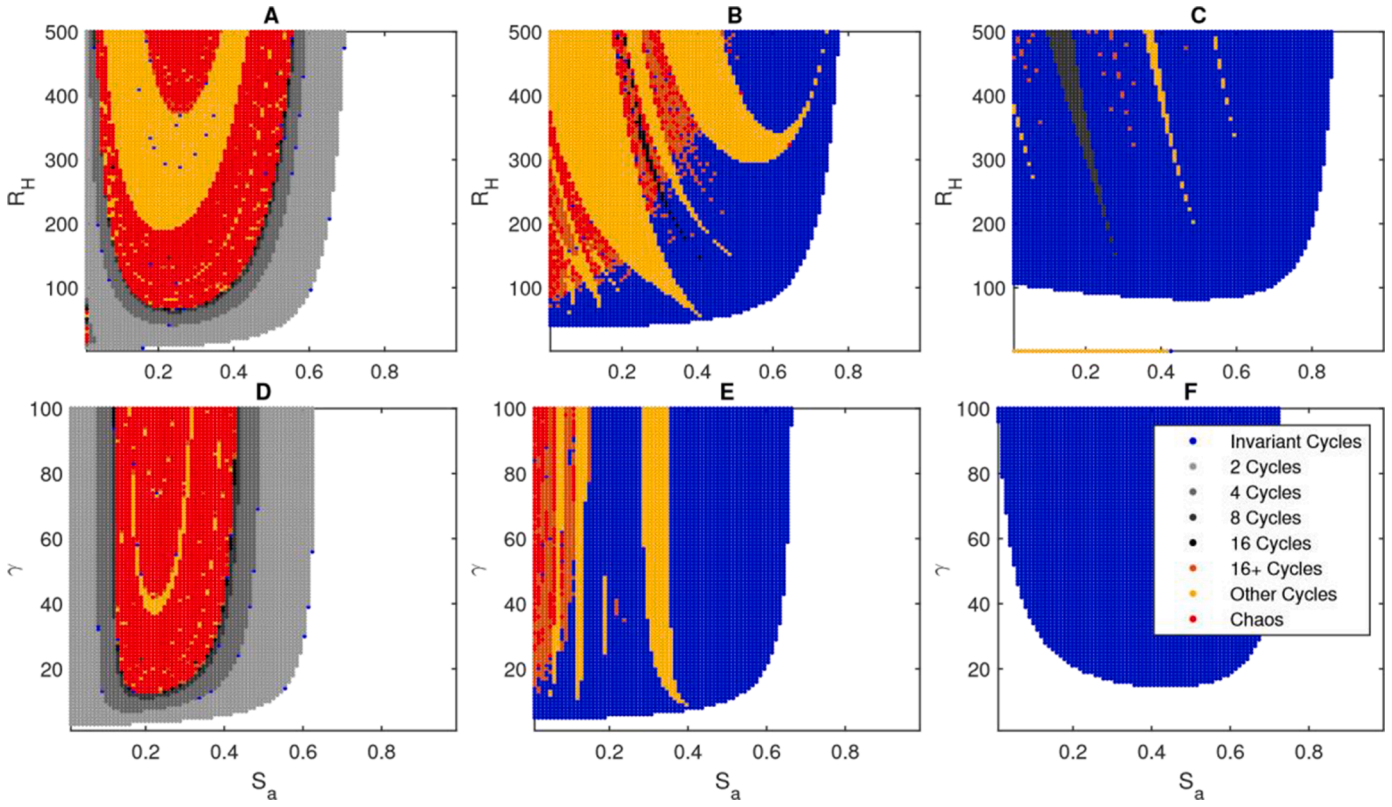

Fig. 4. Attractor planes for a range of adult survival (S_a), yearly recruitment rate (R_H), and densitydependent exponent (γ) for the one-patch model. Attractor type is determined with the Lyapunov exponent with subclassification of k-cycles into 2, 4, 8, 16, 16+ period cycles, and all other k-cycles with less than 16 points (other cycles). Flip bifurcations create k-cycles in the 1-stage model where chaos arises under period-doubling routes with periodic windows of low-point k-cycles. For the 2- and 3-stage models, invariant cycles are created through a Hopf bifurcation with phase-locked regions generating low-point k-cycles in the 3-stage model and a mix of low-point cycles, high-point cycles, and chaos in the 2-stage model.

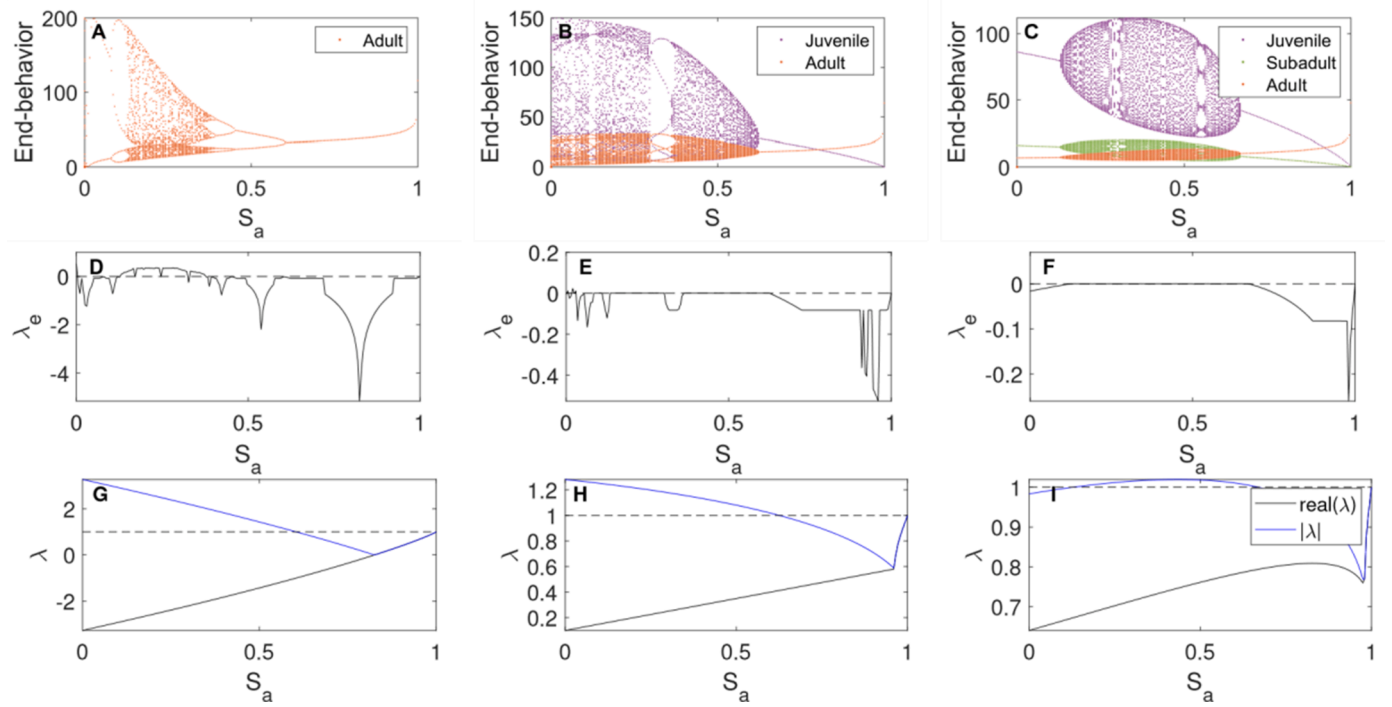

Fig. 5. One-patch bifurcation diagrams (A, B, C) with calculated Lyapunov exponents (D, E, F) and dominant eigenvalues (G, H, I) allow us to analyze bifurcations under a range of adult survival probabilities. In the 1-stage model, k-cycles occur through a flip bifurcation, creating chaos through a period-doubling route. In the 2-stage model, Hopf bifurcations create invariant cycles with phase-locked k-cycles whereas invariant cycles persist in the 3-stage model. Bifurcations and attractor types are verified with respective Lyapunov exponents (2nd row) and dominant eigenvalues (3rd row).

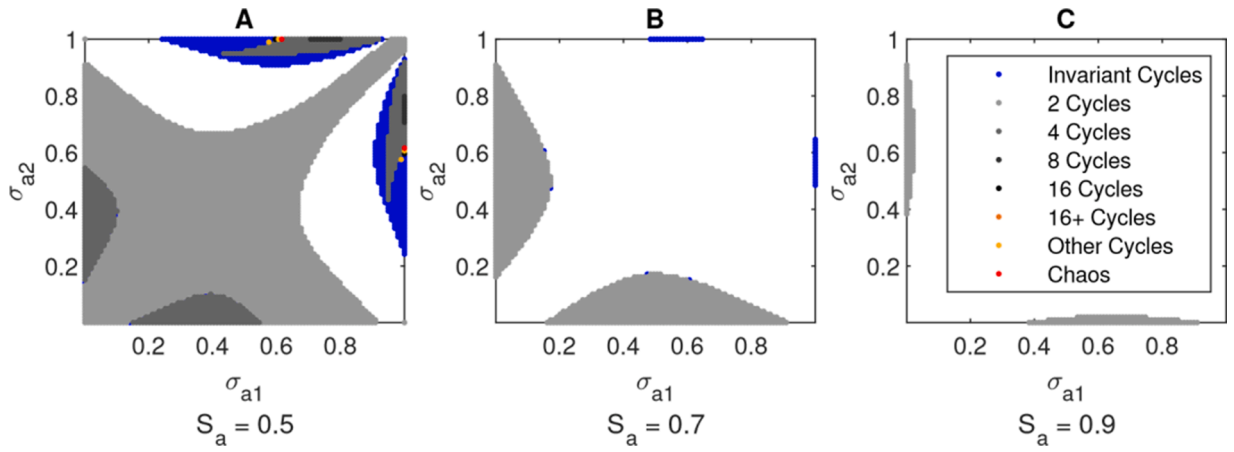

Fig. 6. Attractor planes for homogeneous metapopulations ($S_{a1} = S_{a2}$) in the one stage model show that dispersal regions containing oscillations are similar under small vital rate perturbations. Attractor type is classified as equilibria (white), invariant cycles (blue), k-cycles (black), and chaos (red). K-cycles are further classified based on their periodicity. Dispersal-induced oscillations occur for high adult survival (B, C) in similar unstable regions as intermediate adult survival (A).

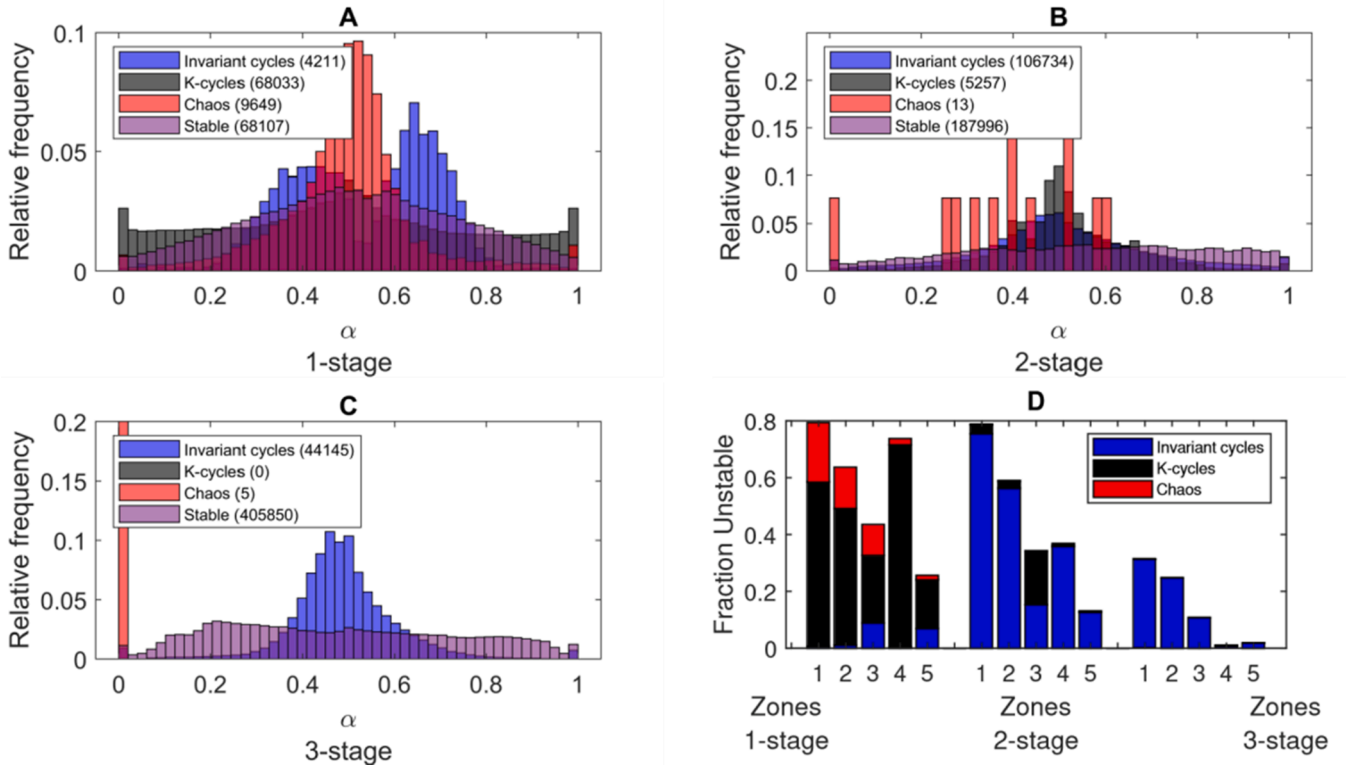

Fig. 7. The relative frequency of per capita symmetric dispersal (α) for each attractor type for the 1-stage (A), 2-stage (B), and 3-stage (C) models, and the fraction that each dispersal type appears in each zone (D). Unstable occurrences are classified as invariant cycles (blue), k-cycles (black), chaos (red), and stable equilibria (purple). The number of occurrences for each attractor type are noted in parentheses. Chaos is most prevalent under symmetric dispersal in the 1-stage model, invariant cycles occur under asymmetric dispersal in the 1-stage model and symmetric dispersal in the 2- and 3-stage models, and k-cycles occur for all dispersal symmetries in the 1-stage model, under high symmetric dispersal in the 2-stage model, and rarely in the 3-stage model. Stable equilibria are present for all symmetries across all models.

the number of invariant and k-cycles.

To summarize population synchrony (β), we plot synchrony histograms for each attractor type in each zone (Fig. 8). For example, of the 2498 1-stage simulations with low symmetric dispersal (top left panel in Fig. 8), 20 exhibited invariant cycles with ~ 80% being perfectly synchronized (blue), 1824 exhibited k-cycles with ~ 70% being perfectly synchronized (black), and 654 exhibited chaos with synchrony being mostly between 0.8 and 1 (red). Across all three life-history stage models, zone 1 has the most mixed results due to low dispersal probabilities from local populations (first row). As dispersal increases, we find more consistency within each zone. For the 1-stage model, higher dispersal regions (zones 2, 3, and 5) have consistently lower synchrony than lower dispersal zones (zones 1 and 4). For the 2-stage model, invariant cycles maintain near-perfect synchrony across all zones. The few instances of chaos either have perfect or intermediate synchrony ($\beta \approx 0.5$), and k-cycles occur with very low synchrony in zone 3 and high synchrony in all other zones. For the 3-stage model, we find consistently high synchrony for all unstable points including a few

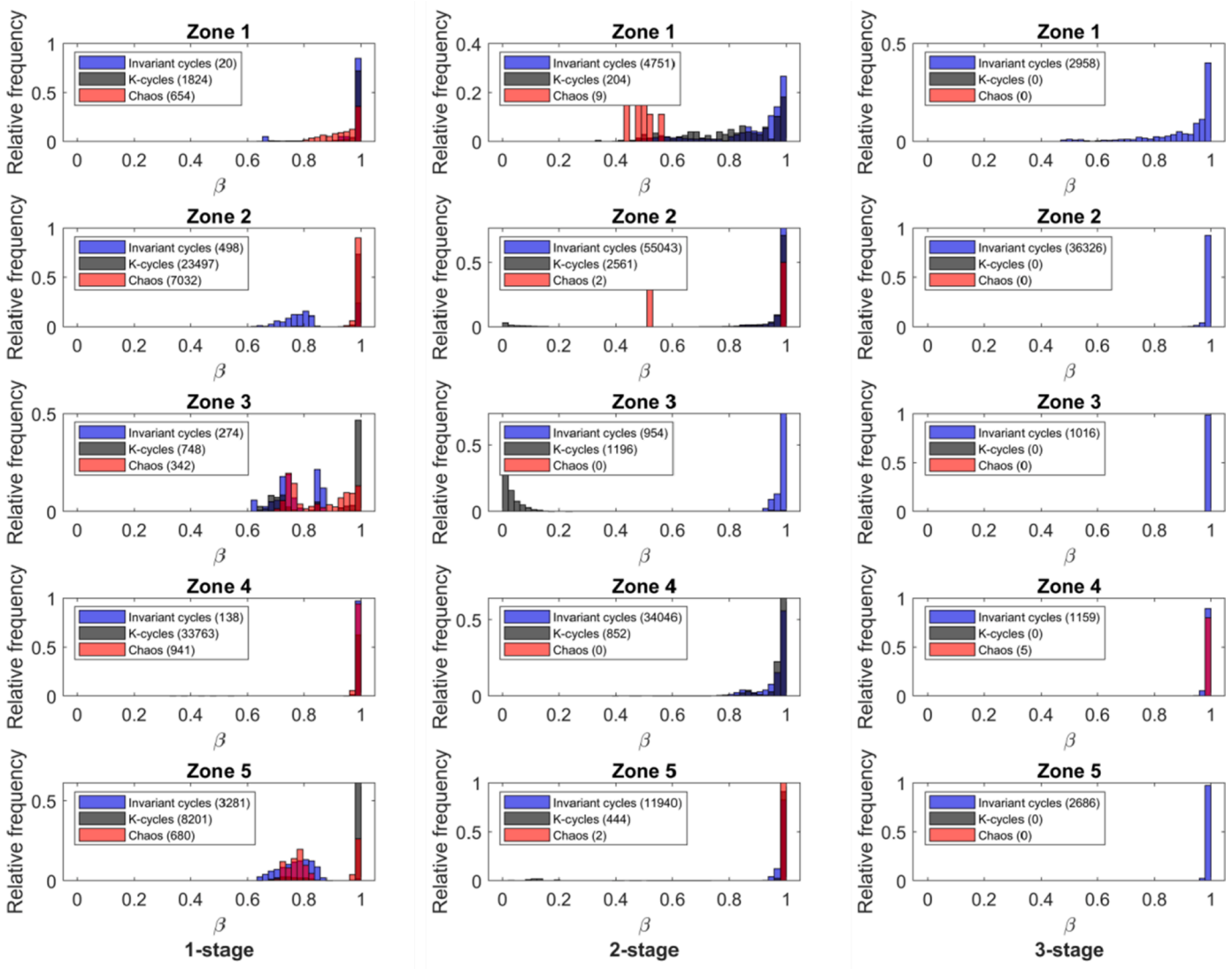

Fig. 8. The relative frequencies for synchrony levels for each attractor type summarize the relationships between synchrony and attractor type in the different dispersal zones. The number of occurrences that an attractor type appears in each zone is in parentheses and β is the proportion of synchrony occurrences within each attractor type. In the 1-stage model, intermediate to high dispersal probabilities (zones 2, 3, and 5) produce lower synchrony ($\beta \approx 0.8$) for all attractor types whereas low dispersal probabilities (zones 1 and 4) have more results with near-perfect synchrony. In the 2-stage model, most results have near-perfect synchrony under sufficient dispersal (zones 2, 3, and 5) with the unique finding of near-perfect asynchronous k-cycles under very high symmetric dispersal (zone 3). In the 3-stage model, highly synchronous invariant cycles are consistently high across all zones.

instances of chaos.

Overall, low and high symmetric dispersal (zones 1 and 3) produce the most variety in synchrony and attractor type, especially for the 1- and 2-stage models. The variety in zone 1 can be expected since they are reflective of local population dynamics without dispersal. However, high symmetric dispersal (zone 3) may cause rapid shifts to oscillations, producing a relatively high number of chaos events in the 1-stage model and low-synchrony k-cycles in the 2-stage model. The latter result is especially interesting since these are the only instances that we see such low synchrony.

3.4. Bifurcation analysis of the two-patch model

The results in the previous section only capture trajectories of one steady state even though multiple steady states may exist. We use bifurcation and eigenvalue plots of select dispersal probabilities to analyze some of the alternate attractors and fixed points that appear in the two-patch model (Figs. 9 and 10). For each σ_{a1} value, we find all nontrivial fixed points by numerically solving for $\boldsymbol{u}_n^* = \boldsymbol{A}_n^* \boldsymbol{u}_n^*$ using trust-region root-finding techniques with 200 randomly selected start conditions (Coleman and Li 1996). See the appendix for details. We use these fixed points to numerically compute eigenvalues for local stability analysis. To identify all attractors for each σ_{a1} value, we initialize simulations with 100 random initial conditions and run the two-patch model for 1000 time steps. This ensures that populations start within the basins of attraction for each unique attractor.

In plots A-C, we represent attractors at chosen σ_{a1} values by plotting the population size of adults in patch 1 for the final 50 time steps (black dots). Additionally, we plot all numerically solved fixed points for each σ_{a1} (red circles). For each fixed point, we plot the real part (black circles) and magnitude (blue dots) of the dominant eigenvalue in plots D-F. Trajectories near unstable fixed points ($|\lambda| > 1$) will converge to one of the attractors, and we identify local bifurcations and alternate steady states by closely inspecting the bifurcation and eigenvalue plots. Note that we do not attempt to identify unstable limit cycles as it requires systematic analysis of global dynamics and bifurcations. We select 3 scenarios in the two-patch, 1-stage model, 2 scenarios in the 2-stage model, and 1 scenario in the 3stage model to show some of the

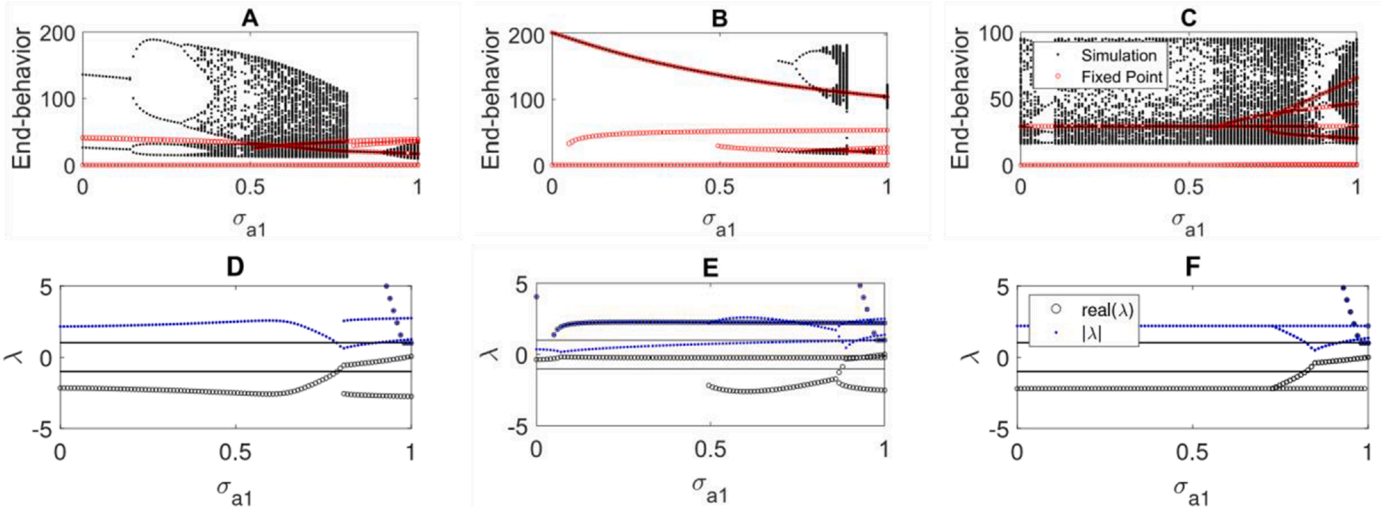

Fig. 9. Bifurcation and eigenvalue plots of all global attractors (black dots), fixed points (red circles), and dominant eigenvalues of fixed points for the two-patch, 1-stage model. As σ_{a1} increases in plots A, D, k-cycles undergo a period-doubling route to chaos ($\sigma_{a1} \approx 0.45$) which then experiences a crisis at $\sigma_{a1} \approx 0.8$, creating a brief window of stability as it collides with an unstable orbit. At $\sigma_{a1} \approx 0.9$, the stable equilibrium undergoes a Hopf bifurcation, creating an invariant cycle. In plots B, E, a k-cycle appears at $\sigma_{a1} \approx 0.7$ and undergoes a period-doubling route to chaos. This persists until a new fixed point is created at $\sigma_{a1} \approx 0.87$. The new fixed point quickly undergoes a flip bifurcation to Hopf bifurcation, causing the alternate attractor to shift from a k-cycle to equilibrium to invariant cycle. In plots C, F, chaos persists under phase-locked k-cycles for $0.15 < \sigma_{a1} < 0.9$ with a period doubling route occurring at $\sigma_{a1} \approx 0.1$. Two unstable fixed points are created at $\sigma_{a1} \approx 0.75$ via a pitchfork bifurcation where only the chaotic attractor exists. The fixed points gain stability for a brief window before once again losing stability via Hopf bifurcations where invariant cycles are created that quickly phase-lock to chaos (see appendix). Parameters used are $S_{a1} = 0.1$, $S_{a2} = 0.3$, $\sigma_{a2} = 0.6$ for plots A, D, $S_{a1} = 0.1$, $S_{a2} = 0.3$, $\sigma_{a2} = 0.96$ for plots B, E, and $S_{a1} = S_{a2} = 0.3$, $\sigma_{a2} = \sigma_{a1}$ for plots C, F.

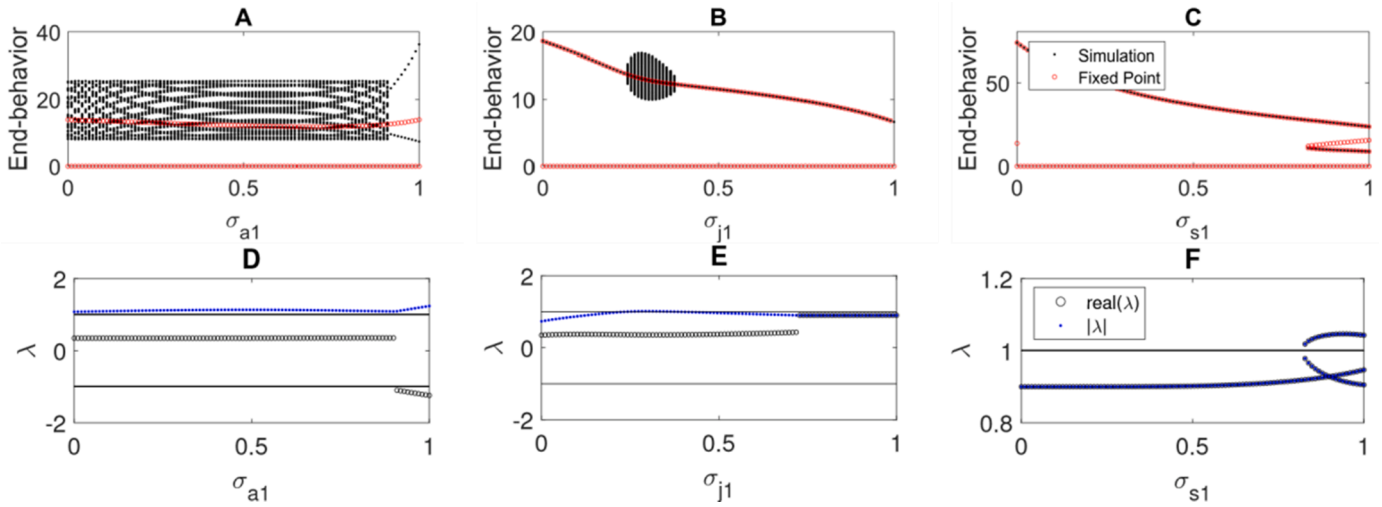

Fig. 10. Bifurcation and eigenvalue plots of all global attractors (black dots), fixed points (red circles), and dominant eigenvalues of fixed points for the two-patch, 2-stage model (columns 1 and 2), and 3-stage model (column 3). In plots A, D, an invariant cycle persists until the loss of the imaginary component in the dominant eigenvalue shifts the invariant cycle to a 2-point k-cycle. In plots B, E, a Hopf bifurcation marks the creation of an invariant cycle for a brief window at $0.3 < \sigma_{j1} < 0.4$ with a stable equilibrium occurring elsewhere. In plots C, F, a saddle-node bifurcation creates two fixed points at $\sigma_{s1} \approx 0.8$, one of which is stable, resulting in two stable nontrivial fixed points. Parameters used are $S_{a1} = S_{a2} = 0.5$, $\sigma_{a2} = \sigma_{a1}$ for plots A, D, $S_{a1} = 0.5$, $S_{a2} = 0.9$, $\sigma_{j2} = 0.8$ for plots B, E, and $S_{a1} = S_{a2} = 0.9$, $\sigma_{s2} = 0.9$ for plots C, F.

different bifurcations that occur in our simulations. All parameters are fixed except for σ_{a2} which may either be fixed or equal to σ_{a1}.

In Fig. 9A, D, a 2-cycle begins for low σ_{a1} that experiences a period-doubling route to chaos at $\sigma_{a1} \approx 0.25$. This persists until it undergoes a crisis at $\sigma_{a1} \approx 0.8$, creating a sudden shift to a stable equilibrium. The stable fixed point undergoes a Hopf bifurcation creating an invariant cycle at $\sigma_{a1} \approx 0.9$. In plots B, E, a stable equilibrium persists throughout the σ_{a1} range and coexists with a k-cycle that is produced through a 2-cycle saddle-node bifurcation at $\sigma_{a1} \approx 0.7$. The k-cycle experiences a period-doubling route to chaos that is suddenly destroyed at $\sigma_{a1} \approx 0.87$ via a crisis. Here, a new fixed point is created that quickly experiences a flip bifurcation, creating a stable equilibrium. The fixed point then undergoes a Hopf bifurcation, causing the birth of an invariant cycle that appears for a small window. Finally, in plots C, F, chaos induced by period-doubling routes persist for $0.15 < \sigma_{a1} < 0.9$. An unstable fixed point appears at $\sigma_{a1} \approx 0.6$ ($|\lambda| > 5$), and a pitchfork bifurcation occurs at $\sigma_{a1} \approx 0.75$ creating two unstable fixed points. As σ_{a1} increases, the unstable fixed points gain stability for a brief window before Hopf bifurcations cause the two stable equilibria to lose stability, creating invariant cycles that quickly become chaotic attractors. The qualitative behavior of the attractors in columns 2 and 3 are verified with phase planes and iteration maps for select σ_{a1} in the appendix.

Fig. 10 shows bifurcation plots and dominant eigenvalues for the 2-stage model (columns 1 and 2) and the 3-stage model (column 3). In plots A, D, we find that an invariant cycle with constant amplitude persists until $\sigma_{a1} \approx 0.9$ where the dominant eigenvalue loses its imaginary component while the real component is less than -1. This creates a sudden shift from invariant cycles to 2-point k-cycles with increasing amplitude as σ_{a1} increases. Plots B, E show a small window of invariant cycles occurring for $0.3 < \sigma_{j1} < 0.4$, and another destruction of the imaginary component of the dominant eigenvalue occurring at $\sigma_{j1} \approx 0.65$, shifting the fixed point from a stable spiral to a stable node. Finally, in plots C, F, a stable equilibrium persists for all σ_{s1} while a saddle-node bifurcation occurs at $\sigma_{s1} \approx 0.8$, creating asymptotically stable and unstable fixed points.

4. Discussion

In this paper, we used stage-structured matrix models with density-dependent first-year survival to analyze the effects of dispersal in a two-patch system of a species with 1, 2, and 3 life-history stages. We used eigenvalue, bifurcation, and Lyapunov exponent analyses to identify qualitative shifts in dynamics and the bifurcations surrounding these shifts. We observed a variety of bifurcation types and routes to chaos, including period-doubling, phase-locking, and crisis. Where previous studies have investigated the relationship between synchrony and population variance (Abbott 2011; Allen et al. 1993; Jansen 1999; Wang et al. 2015), or the effects of dispersal on shifts in dynamics (Abbott 2011; Amarasekare 1998; Ives et al. 2003; Wang et al. 2015; Wang and Loreau 2014; Ylikarjula et al. 2000), analyzing the relationship between oscillation type and synchrony has not been done before. Our result that populations experiencing chaotic fluctuations are not necessarily less synchronized than other oscillation types challenges previous studies that assume chaos is associated with low population synchrony.

We assumed constant dispersal probabilities though different dynamics may result under different dispersal rules (Amarasekare 1998; Kendall and Fox 1998; Ruxton 1996; Ylikarjula et al. 2000). For example, Ylikarjula et al. (2000) found a variety of results when testing both density-dependent and density-independent dispersal; however, they did not find any general differences between the two dispersal types on population variance. On the other hand, Amarasekare (1998) found that strong density-dependent dispersal increased the tendency towards complex dynamics. The consequences of dispersal strategies are seemingly sensitive to model characteristics, including density-dependent dispersal type, dispersal mortality, demographic density-dependence type, and growth rates (Amarasekare 1998; Ripa 2000; Ylikarjula et al. 2000). Even with simple dispersal assumptions, we found complicated dynamics in our results, but these are expected to change under different dispersal behavior and rules.

We found that constant dispersal had a nonlinear effect on population synchrony. Specifically, low dispersal probabilities initially synchronized populations while moderate to high dispersal may rapidly desynchronize populations. This was found for high asymmetric dispersal in the one-stage model and high symmetric dispersal in the two-stage model. Asymmetric dispersal has been shown to decrease synchrony in especially one-directional dispersal patterns (Doebeli 1995). Dispersal type and the number of patches in a metapopulation seemingly play a large role on synchrony (Kendall and Fox 1998; Ylikarjula et al. 2000). Ylikarjula et al. (2000) found that different dispersal rules produce a variety of results in the two-patch model but have less of an effect on population synchrony when the number of patches is increased. Therefore, care should be taken when extrapolating our results to metapopulations with a higher number of patches.

We assumed that population fluctuations were driven by density-dependent demographic processes. However, fluctuations, and consequently synchrony, could be influenced by environmental processes (Ranta et al. 1997). In fact, Ripa (2000) argues that the Moran effect is ever-present and should not be discounted when analyzing the synchrony-dispersal relationship. The effects of dispersal on population synchrony then depend on the degree of correlated stochasticity and fluctuations induced by intrinsic dynamics (Ripa 2000). Because of the nature of cycles induced by demographic processes, it is much easier to maintain synchrony among populations with intrinsically-induced cycles than a system where population fluctuations are driven by uncorrelated stochasticity (Ripa 2000). Therefore, we may expect different results under stochastically-driven fluctuations than fluctuations driven by demographic processes.

Although we did not explicitly define landscape geography, distances between patches can play an important role in metapopulation dynamics (Holland and Hastings 2008). Patches further from each other can create more complex dynamics while decreasing synchrony (Kaneko 1985; Kendall and Fox 1998; Ripa 2000; Bjørnstad et al. 1999). The negative relationship between synchrony and distance agrees with populations driven by environmental change as weather patterns are less correlated at greater distances (Ranta et al. 1999). Similarly, oscillations are more prevalent as distance increases since less dispersal is expected across greater distances. Although outside the scope of this study, it would be interesting to explore the effects of dispersal on different network structures and dispersal strategies.

Chaotic oscillations are typically considered to enhance viability due to naturally noisy dynamics and low synchrony; however, this may only be true for chaos induced by environmental variation with low dispersal rates (Allen et al. 1993; Heino et al. 1997; Ylikarjula et al. 2000). We found that chaos was not necessarily less synchronous than other attractor types. Specifically, chaos was created through one of three mechanisms (period-doubling, phase-locking, and crisis), and synchrony did not experience any sudden shifts throughout these routes to chaos. This means that chaos did not have any desynchronizing effects on population synchrony in our models, and consequently, may not necessarily have the effects on population rescue as previously thought (Allen et al. 1993). That being said, it is not certain that all routes to chaos preserve synchrony, and it would be interesting to explore other routes to chaos to determine whether or not chaos has any desynchronizing effects in deterministic models.

The purpose of this research was to investigate the dynamics of matrix population models relevant for amphibian research (Halley et al. 1996; Vonesh and De la Cruz 2002; Willson et al. 2012; Willson and Hopkins 2013). Although we did not focus on any one species in particular, our results demonstrate that the interactions between dispersal and demography play key roles in determining population dynamics. Amphibian species with rapid maturation may experience more complicated dynamics at varying levels of dispersal as indicated by our models with one life-history stage. Conversely, the dynamics of species with slower development (two to three life-history stages) are less impacted by dispersal, resulting in a higher frequency of equilibrium states and less chaos. We present this information to encourage further research using these types of models on a particular species of interest, noting the importance of accurately identifying amphibian life histories and dispersal processes. This helps facilitate effective strategies that can be used for conservation management action.

CRediT authorship contribution statement

Guenchik Grosklos and Jia Zhao conceived the ideas and designed the methodology. Guenchik Grosklos performed the simulations and led the analysis. Guenchik Grosklos wrote the manuscript, and Jia Zhao edited it.

Data accessibility

All data sets are made available in supplementary materials.

Declaration of Competing Interest

The authors declare that they have no known competing financial interests or personal relationships that could have appeared to influence the work reported in this paper.

Data availability

No data was used for the research described in the article.

Acknowledgments

Funding and support provided in part by the National Science Foundation under Grant No. 1633756. G.G. and J.Z. would also like to acknowledge the support of NSF-DMS-1816783.

Supplementary materials

Supplementary material associated with this article can be found, in the online version, at doi:10.1016/j.ecolmodel.2022.110203.

References

Abbott, K., 2011. A dispersal-induced paradox: synchrony and stability in stochastic metapopulations. Ecol. Lett. 14, 1158–1169.
Allen, J., Shaffer, W., Rosko, D., 1993. Chaos reduces species extinction by amplifying local population noise. Nature 364, 229–232.
Amarasekare, P., 1998. Interactions between local dynamics and dispersal: insights from single species models. Theor. Popul. Biol. 53, 44–59.
Anazawa, M., 2019. Inequality in resource allocation and population dynamics models. R. Soc. Open Sci. 6, 1–11.
Bendik, N.F., Dries, L.A., 2018. Density-dependent and density-independent drivers of population change in barton springs salamanders. Nat. Ecol. Evol. 8, 5912–5923.
Biek, R., Funk, W., Maxell, B., Mills, L., 2002. What is missing in amphibian decline research: insights from ecological sensitivity analysis. Conserv. Biol. 16, 728–734.
Bjørnstad, O.N., Ims, R.A., Lambin, X., 1999. Spatial population dynamics: analyzing patterns and processes of population synchrony. TREE 14, 427–432.
Boualit, L., Pichenot, J., Besnard, A., Helder, R., Joly, P., Cayuela, H., 2019. Environmentally mediated reproductive success predicts breeding dispersal decisions in an early successional amphibian. Anim. Behav. 149, 107–120.
Bowler, D.E., Benton, T.G., 2005. Causes and consequences of animal dispersal strategies: relating individual behaviour to spatial dynamics. Biol. Rev. Camb. Philos. Soc. 80, 205–225.
Băncilă, R.I., Ozgul, A., Hartel, T., Sos, T., Schmidt, B.R., 2016. Direct negative density-dependence in a pond-breeding frog population. Ecography 39, 449–455.
Bull, E. 2005. Ecology of the columbia spotted frog in northeastern oregon. Tech. rep., USDA Forest Service, Pacific Northwest Research Station.
Buxton, V.L., Sperry, H., 2017. A review of how predation and competition affects the deposition of eggs and tadpoles. Bioscience 67, 26–38.
Caswell, H. 2001. Matrix population models – construction, analysis, and interpretation. Sinauer Associates, Inc., Sunderland, Massachusetts.
Cayuela, H., Schmidt, B.R., Weinbach, A., Besnard, A., Joly, P., 2018. Multiple densitydependent processes shape the dynamics of a spatially structured amphibian population. J. Anim. Ecol. 88, 164–177.
Cayuela, H.A. Valenzuela-Sanchez, L. Teulier, I.N. Martínez-Solano, J.P.Lena, J. Merila, E. Muths, R. Shine, L. Quay, Denoël, J. Clobert, and B.R. Schmidt. 2020. Determinants and consequences of dispersal in vertebrates with complex life cycles: a review of pondbreeding amphibians.
Coleman, T.F., Li, Y., 1996. An interior, trust region approach for nonlinear minimization subject to bounds. SIAM J. Optim. 6, 418–445.
Dey, S., Goswami, B., Joshi, A., 2014. Effects of symmetric and asymmetric dispersal on the dynamics of heterogeneous metapopulations: two patch systems revisited. J. Theor. Biol. 345, 52–60.
Doebeli, M., 1995. Dispersal and dynamics. Theor. Popul. Biol. 47, 82–106.
Funk, W., Greene, A., Corn, P., Allendorf, F., 2005. High dispersal in a frog species suggests that it is vulnerable to habitat fragmentation. Biol. Lett. 1, 13–16.
Gamble, L.R., McGarigal, K., Compton, B.W., 2007. Fidelity and dispersal in the pondbreeding amphibian, *Ambystoma opacum*: Implications for spatio-temporal population dynamics and conservation. Biol. Conserv. 139, 247–257.
Gyllenberg, M., Söderbacka, G., Ericsson, S., 1992. Does migration stabilize local population dynamics? analysis of a discrete metapopulation model. Math. Biosci. 118, 25–49.
Halley, J.M., Oldham, R., Arntzen, J., 1996. Predicting the persistence of amphibian populations with the help of a spatial model. J. Appl. Ecol. 33, 455–470.
Hassell, M.P., 1975. Density-dependence in single-species populations. J. Anim. Ecol. 44, 283–295.
Hastings, A., 2004. Transients: the key to long-term ecological understanding? Trends Ecol. Evol. 19, 39–45.
Heino, M., Kaitala, V., Ranta, E., Lindstrom, J., 1997. Synchronous dynamics and rates of extinction in spatially structured populations. Proc. Biol. Sci. 264, 481–486.
Hellriegel, B., 2000. Single- or multistage regulation in complex life cycles: does it make a difference? Oikos 88, 239–249.
Holland, M.D., Hastings, A., 2008. Strong effect of dispersal network structure on ecological dynamics. Nature 456, 792–795.
Hudson, P.J., Cattadori, I.M., 1999. The moran effect: a cause of population synchrony. TREE 14, 1–2.
Ives, A.R., Dennis, B., Cottingham, K.L., Carpenter, S.R., 2003. Estimating community stability and ecological interactions from time-series data. Ecol. Monogr. 73, 301–330.
Jansen, V.A., 1999. Phase locking: another cause of synchronicity in predator-prey systems. TREE 14, 278–279.
Kaneko, K., 1985. Spatial period-doubling in open flow. Phys. Lett. 111, 321–325.
Kendall, B.E., Fox, G.A., 1998. Spatial structure, environmental heterogeneity, and population dynamics: analysis of the coupled logistic map. Theor. Popul. Biol. 54, 11–37.
Loreau, M., Mazancourt, C.d., 2008. Species synchrony and its drivers: Neutral and noneutral community dynamics in fluctuating environments. Am. Nat. 172, 48–66.
McCaffery, R., Eby, L., Maxell, B., Corn, P., 2014. Breeding site heterogeneity reduces variability in frog recruitment and population dynamics. Biol. Conserv. 170, 169–176.
McCaffery, R., Maxell, B., 2010. Decreased winter severity increases viability of a montane frog population. Proc. Natl. Acad. Sci. U. S. A. 9, 8644–8649.
McCaffery, R., Solonen, A., Crone, E., 2012. Frog population viability under present and future climate conditions: a bayesian state-space approach. J Anim. Ecol. 81, 978–985.
Moran, P.A.P., 1953. The statistical analysis of the canadian lynx cycle. II. synchronization and meteorology. Aust. J. Zool. 1, 291–298.
Patla, D., and D. Keinath. 2005. Columbia spotted frog (*Rana luteiventris* formerly *R. pretiosa*): A technical conservation assessment. Tech. rep., USDA Forest Service, Rocky Mountain Region.
Ranta, E., Kaitala, V., Lindström, J., 1997. The moran effect and synchrony in population dynamics. Oikos 78, 136–142.
Ranta, E., Kaitala, V., Lindström, J., 1999. Spatially autocorrelated disturbances and patterns in population synchrony. Proc. R. Soc. B 266, 1851–1856.
Ranta, E., Kaitala, V., Lundberg, P., 1998. Population variability in space and time: the dynamics of synchronous population fluctuations. Oikos 83 (2), 376–382. No.
Reaser, J., 2000. Demographic analysis of the columbia spotted frog (*Rana luteiventris*): case study in spatiotemporal variation. Can. J. Zool. 78, 1158–1167.
Ripa, J., 2000. Analysing the moran effect and dispersal: significance and interaction in synchronous population dynamics. Oikos 90, 175–187.
Ross, D.A., Reaser, J.K., Kleeman, P., Drake, D.L., 1999. *Rana luteiventris*. (columbia spotted frog) mortality and site fidelity. Herpetol. Rev. 30, 163.
Ruxton, G.D., 1996. Density-dependent migration and stability in a system of linked populations. Bull. Math. Biol. 58, 643–660.
Semlitsch, R.D., 2010. Differentiating migration and dispersal processes for pond-breeding amphibians. J. Wildl. Manag. 72, 260–267.
Strogatz, S.H., 2015. Nonlinear dynamics and chaos, 2nd ed. Westview Press, Boulder, Colorado.
Tournier, E., Besnard, A., Tournier, V., Cayuela, H., 2017. Manipulating waterbody hydroperiod affects movement behaviour and occupancy dynamics in an amphibian. Freshw. Biol. 62, 1768–1782.
Udwadia, F.E., Raju, N., 1998. Some global properties of a pair of coupled maps. Phys. D 111, 16–26.
Vonesh, J.R., De la Cruz, O., 2002. Complex life cycles and density dependence: assessing the contribution of egg mortality to amphibian declines. Oecologia 133, 325–333.
Wang, S., Haegeman, B., Loreau, M., 2015. Dispersal and metapopulation stability. PeerJ 3, 1–16.
Wang, S., Loreau, M., 2014. Ecosystem stability in space: α, β, and γ variability. Ecol. Lett. 17, 891–901.
Willson, J.D., Hopkins, W.A., 2013. Evaluating the effects of anthropogenic stressors on source-sink dynamics in pond-breeding amphibians. Conserv. Biol. 27, 595–604.
Willson, J.D., Hopkins, W.A., Bergeron, C.M., Todd, B.D., 2012. Making leaps in amphibian ecotoxicology: translating individual-level effects of contaminants to population viability. Ecol. Appl. 22, 1791–1802.
Ylikarjula, J., Alaja, S., Laakso, J., Tesar, D., 2000. Effects of patch number and dispersal patterns on population dynamics and synchronyl. J. Theor. Biol. 207, 377–387.